Inorganic Chemistry
Article

Inorg. Chem. **2010**, *49*, 10455–10467 **10455**
DOI: 10.1021/ic101474e

Structural, Electronic, and Magnetic Properties of $UFeS_3$ and $UFeSe_3$

Geng Bang Jin,[†] Emilie Ringe,[†] Gary J. Long,*[,‡] Fernande Grandjean,[§] Moulay T. Sougrati,[§] Eun Sang Choi,[∥] Daniel M. Wells,[†] Mahalingam Balasubramanian,[⊥] and James A. Ibers*[,†]

[†]*Department of Chemistry, Northwestern University, 2145 Sheridan Road, Evanston, Illinois 60208-3113, United States,* [‡]*Department of Chemistry, Missouri University of Science and Technology, University of Missouri, Rolla, Missouri 65409-0010, United States,* [§]*Department of Physics, B5, University of Liège, B-4000 Sart Tilman, Belgium,* [∥]*Department of Physics and the National High Magnetic Field Laboratory, Florida State University, Tallahassee, Florida 32310, United States, and* [⊥]*Advanced Photon Source, Argonne National Laboratory, Argonne, Illinois 60439, United States*

Received July 23, 2010

Black prisms of $UFeS_3$ and $UFeSe_3$ have been synthesized by solid-state reactions of U, Fe, and S or Se with CsCl as a flux at 1173 K. The structure of these isostructural compounds consists of layers of edge- and corner-sharing FeS_6 or $FeSe_6$ octahedra that are separated by layers of face- and edge-sharing US_8 or USe_8 bicapped trigonal prisms. The isomer shifts in the iron-57 Mössbauer spectra of both $UFeS_3$ and $UFeSe_3$ are consistent with the presence of high-spin iron(II) ions octahedrally coordinated to S or Se. The XANES spectra of $UFeS_3$ and $UFeSe_3$ are consistent with uranium(IV). Single-crystal magnetic susceptibility measurements along the three crystallographic axes of $UFeSe_3$ reveal a substantial magnetic anisotropy with a change of easy axis from the *a*-axis above 40 K to the *b*-axis below 40 K, a change that results from competition between the iron(II) and uranium(IV) anisotropies. The temperature dependence of the magnetic susceptibility along the three axes is characteristic of two-dimensional magnetism. A small shoulder-like anomaly is observed in the magnetic susceptibilities along the *a*- and *b*-axes at 96 and 107 K, respectively. Below 107 K, the iron-57 Mössbauer spectra of $UFeS_3$ and $UFeSe_3$ show that the iron nuclei experience a magnetic hyperfine field that results from long-range magnetic ordering of at least the iron(II) magnetic moments because the field exhibits Brillouin-like behavior. Below 40 K there is no significant change in the Mössbauer spectra as a result of change in magnetic anisotropy. The complexity of the iron-57 Mössbauer spectra and the temperature and field dependencies of the magnetic properties point toward a complex long-range magnetic structure of two independent iron(II) and uranium(IV) two-dimensional sublattices. The temperature dependence of the single-crystal resistivity of $UFeSe_3$ measured along the *a*-axis reveals semiconducting behavior between 30 and 300 K with an energy gap of about 0.03 eV below the 53 K maximum in susceptibility, of about 0.05 eV between 50 and 107 K, and of 0.03 eV above 107 K; a negative magnetoresistance was observed below 60 K.

Introduction

An interaction between actinide 5f orbitals and transition-metal 3d-orbitals often leads to interesting electronic and magnetic properties. Single-crystal studies have recently been performed on numerous actinide transition-metal chalcogenide compounds with the aid of the better synthetic and analytical techniques developed over the last few decades.[1−5]

The ternary phases of the general stoichiometry $AnMQ_3$ (An = U or Th; M = transition metal; Q = S, Se, or Te) are among some of the most studied compounds, primarily because of their simple and robust structures. These compounds crystallize in a distorted perovskite-type structure with An occupying eight-coordinate interstitial sites within a framework of MQ_6 octahedra. Many of the $AnMQ_3$ compounds adopt a three-dimensional structure in space group *Pnma*.[1] However, when M is Sc, Fe, or Mn, the compounds adopt a two-dimensional layered structure in space group *Cmcm*.[2,4,6−9] Interestingly, based on both the U−Q interatomic distances and charge balance, uranium appears to be

*To whom correspondence should be addressed. E-mail: glong@mst.edu (G.J.L.), ibers@chem.northwestern.edu (J.A.I.).

(1) Narducci, A. A.; Ibers, J. A. *Chem. Mater.* **1998**, *10*, 2811–2823.
(2) Narducci, A. A.; Ibers, J. A. *Inorg. Chem.* **2000**, *39*, 688–691.
(3) Huang, F. Q.; Mitchell, K.; Ibers, J. A. *Inorg. Chem.* **2001**, *40*, 5123–5126.
(4) Ijjaali, I.; Mitchell, K.; Huang, F. Q.; Ibers, J. A. *J. Solid State Chem.* **2004**, *177*, 257–261.
(5) Burgaris, D. E.; Ibers, J. A. *Dalton Trans.* **2010**, *39*, 5949–5964.
(6) Julien, R.; Rodier, N.; Tien, V. *Acta Crystallogr., Sect. B: Struct. Crystallogr. Cryst. Chem.* **1978**, *34*, 2612–2614.
(7) Noël, H.; Padiou, J.; Prigent, J. *C. R. Séances Acad. Sci., Ser. C* **1971**, *272*, 206–208.
(8) Noël, H. *C. R. Séances Acad. Sci., Ser. C* **1974**, *279*, 513–515.
(9) Noël, H.; Padiou, J. *Acta Crystallogr., Sect. B: Struct. Crystallogr. Cryst. Chem.* **1976**, *32*, 1593–1595.

Published on Web 10/21/2010

trivalent[6] in $UScS_3$ and tetravalent[4,7−9] in UMQ_3 (M = Fe or Mn; Q = S or Se), even though the compounds are isostructural. To date there has been little progress in understanding the origin of, or even confirming, the different oxidation states that uranium displays in these compounds. For instance, when M is Sc, Fe, or Mn, only the magnetic properties of $UMnSe_3$[4] and $ThMnTe_3$[2] have been determined; these reveal that the compounds are ferromagnetic with Curie temperatures, T_C, of 62 and 70 K, respectively.

Both $UFeS_3$ and $UFeSe_3$ were first synthesized and structurally characterized[7−9] more than three decades ago but, surprisingly, none of their physical properties have been reported to date. However, some of their related uranium−iron chalcogenide compounds exhibit very unusual magnetic properties. Specifically, U_2FeS_5 has a relatively high T_C of 250 K, a value that results from Fe−Fe magnetic-exchange coupling;[10] the U−Fe and U−U magnetic-exchange interactions become significant only at lower temperatures. As a result of the competing magnetic-exchange pathways, both a reorientation of the antiferromagnetic iron moments and a sharp increase in the canted uranium 5f moment occur between 18 and 25 K. In contrast, U_8FeS_{17} and U_8FeSe_{17} order antiferromagnetically at 47 and 67 K, respectively.[11]

When compared to U_2FeS_5, U_8FeS_{17}, or U_8FeSe_{17}, both $UFeS_3$ and $UFeSe_3$ have simpler, higher symmetry structures as well as a higher concentration of iron. Therefore, we believe it is worthwhile to determine the magnetic interactions between the uranium and iron centers in both $UFeS_3$ and $UFeSe_3$. Thus, we have resynthesized and characterized both $UFeS_3$ and $UFeSe_3$ and herein we report their structures, iron-57 Mössbauer and XANES spectra, and magnetic and electrical properties.

Experimental Section

Syntheses. ^{238}U turnings (Oak Ridge National Laboratory), Fe (Aesar, 99.9%), S (Alfa-Aesar, 99.99%), Se (Cerac 99.999%), Sb (Aldrich, 99.5%), FeSe (Alfa-Aesar, 99.9%), CsCl (Strem Chemicals, 99.999%), NaCl (Fisher, 99.3%), and KCl (Alfa-Aesar, 99.3%) were used as received. Finely divided uranium powder was prepared by a modification of the literature procedure.[12]

The reaction mixtures for $UFeS_3$ and $UFeSe_3$ included 0.06 g of total reactants with U, Fe, and S or Se in a molar ratio of 1:1:3 and 0.13 g of CsCl flux. The preparation of $UFeS_3$ used U (0.037 g, 0.16 mmol), Fe (0.009 g, 0.16 mmol), and S (0.015 g, 0.47 mmol) and that of $UFeSe_3$ used U (0.027 g, 0.11 mmol), Fe (0.006 g, 0.11 mmol), and Se (0.027 g, 0.34 mmol). The reactants were placed in fused-silica ampules in an argon-filled glovebox. Then the ampules were evacuated to about 10^{-4} Torr and flame-sealed. The reaction mixtures were then placed in a computer-controlled furnace and heated to 1173 K in 30 h, maintained at 1173 K for 4 days, cooled to 773 K in 6 days, maintained at 773 K for 2 days, and then cooled to 298 K over 6 h. The reaction products were washed with water and dried with acetone. Selected crystals of each product were examined with both an EDX-equipped Hitachi S-3400 SEM and by X-ray diffraction measurements. Both $UFeS_3$ and $UFeSe_3$ are air stable for a few months.

For the U/Fe/S reaction, the major product was black prisms of $UFeS_3$, but the reaction also produced a small amount of black polyhedral blocks of U_2FeS_5,[13] black US_3 ribbons,[14] black US_2 needles,[15] black Fe_7S_8 prisms,[16] and a red Cs/Fe/S phase. Complete separation of $UFeS_3$ and U_2FeS_5 was very difficult owing to the similar appearance of the products. The combined yield of $UFeS_3$ and U_2FeS_5 was about 90% based on uranium. For the U/Fe/Se reaction, $UFeSe_3$ was the only product obtained, as indicated by optical microscopy and powder X-ray diffraction measurements. The yield was close to 100%. The $UFeSe_3$ crystals are in the form of large black prisms up to a few millimeters in length.

Structure Determinations. Single-crystal X-ray diffraction data for $UFeS_3$ and $UFeSe_3$ were collected with the use of graphite-monochromatized Mo $K\alpha$ radiation (λ = 0.71073 Å). The 80, 100, and 297 K data for $UFeS_3$ were obtained with a Bruker APEX2 diffractometer,[17] whereas the 297 K data for $UFeSe_3$ were obtained with a Bruker Smart-1000 CCD diffractometer.[18] The crystal-to-detector distance was 5.023 cm. Crystal decay was monitored by recollecting 50 initial frames at the end of the data collection. Data were collected by a scan of 0.3° in ω in groups of 606 frames at φ settings of 0°, 90°, 180°, and 270°. The exposure times for $UFeS_3$ and $UFeSe_3$ were 20 and 15 s/frame, respectively.

The collection of intensity data for $UFeS_3$ and $UFeSe_3$ was carried out with the APEX2 program[17] and the SMART program,[18] respectively. Cell refinement and data reduction were carried out with the use of the program APEX2.[17] A Leitz microscope equipped with a calibrated traveling micrometer eyepiece was employed to measure accurately the crystal dimensions. Face-indexed absorption, incident beam, and decay corrections were performed with the use of the program SADABS.[18] The structures were solved with the direct-methods SHELXS program and refined with the full-matrix least-squares SHELXL program.[19] The STRUCTURE TIDY program[20] was used to standardize the positional parameters. Additional experimental details are given in Table 1 and in the Supporting Information.

Powder X-ray Diffraction. Powder X-ray diffraction patterns were collected with a Rigaku Geigerflex powder X-ray diffractometer with the use of Cu $K\alpha$ radiation (λ = 1.5418 Å).

X-ray Absorption Spectroscopy. X-ray absorption near-edge spectral experiments were performed in Sector 20 on the bending magnet beamline, PNC/XOR, 20-BM, at the Advanced Photon Source at Argonne National Laboratory, IL, U.S.A. Measurements at the uranium L_3 edge were performed in the transmission mode at 293 K by using gas ionization chambers to monitor the incident and transmitted X-ray intensities. A third ionization chamber was used in conjunction with a uranyl nitrate standard to provide an internal calibration for the alignment of the edge positions. Monochromatic X-rays were obtained by using a fixed-exit Si (111) double crystal monochromator. A rhodium-coated X-ray mirror was utilized to suppress higher order harmonics. Data reduction was carried out with the Athena software.[21]

(10) Wolfers, P.; Bacmann, M. *Proc. 2nd Int. Con. Electr. Str. Actin.* **1976**, *VI-19*, 483–488.
(11) Noël, H.; Troc, R. *J. Solid State Chem.* **1979**, *27*, 123–135.
(12) Bugaris, D. E.; Ibers, J. A. *J. Solid State Chem.* **2008**, *181*, 3189–3193.
(13) Noël, H.; Potel, M.; Padiou, J. *Acta Crystallogr., Sect. B: Struct. Crystallogr. Cryst. Chem.* **1976**, *32*, 605–606.
(14) Kwak, J. E.; Gray, D. L.; Yun, H.; Ibers, J. A. *Acta Cryst. Sect. E: Struct. Rep. Online* **2006**, *62*, i86–i87.
(15) Suski, W.; Gibinski, T.; Wojakowski, A.; Czopnik, A. *Phys. Status Solidi A* **1972**, *9*, 653–658.
(16) Powell, A. V.; Vaqueiro, P.; Knight, K. S.; Chapon, L. C.; Sánchez, R. D. *Phys. Rev. B* **2004**, *70*, 014415−1–014415−12.
(17) *APEX2, Version 2008.6-1, and SAINT, Version 7.34a, Data Collection and Processing Software*; Bruker Analytical X-Ray Instruments, Inc.: Madison, WI, 2006.
(18) *SMART, Version 5.054, Data Collection and SAINT-Plus, Version 6.45a, Data Processing Software for the SMART System*; Bruker Analytical X-Ray Instruments, Inc.: Madison, WI, 2003.
(19) Sheldrick, G. M. *Acta Crystallogr., Sect. A: Found. Crystallogr.* **2008**, *64*, 112–122.
(20) Gelato, L. M.; Parthé, E. *J. Appl. Crystallogr.* **1987**, *20*, 139–143.

Table 1. Crystal Data and Structural Refinements for $UFeS_3$ and $UFeSe_3$[a]

	$UFeS_3$, 80 K	$UFeS_3$, 100 K	$UFeS_3$, 297 K	$UFeSe_3$, 297 K
formula weight, g/mol	390.06	390.06	390.06	530.76
temperature, K	80(2)	100(2)	297(2)	297(2)
a (Å)	3.7911(1)	3.7905(1)	3.8009(1)	3.9457(8)
b (Å)	11.5746(3)	11.5740(3)	11.6148(4)	12.214(3)
c (Å)	8.6888(2)	8.6880(2)	8.7022(3)	9.121(2)
V (Å^3)	381.27(2)	381.15(2)	384.17(2)	439.6(2)
ρ_c (g cm^{-3})	6.795	6.797	6.744	8.020
μ (cm^{-1})	476.16	476.30	472.56	647.17
$R(F)$[b]	0.0152	0.0152	0.0149	0.0263
$R_w(F^2)$[c]	0.0489	0.0453	0.0430	0.0625

[a] For both structures, $Z = 4$, space group = *Cmcm*, and $\lambda = 0.71073$ Å. [b] $R(F) = \sum||F_o| - |F_c||/\sum|F_o|$ for $F_o^2 > 2\sigma(F_o^2)$. [c] $R_w(F_o^2) = \{\sum w(F_o^2 - F_c^2)^2/\sum wF_o^4\}^{1/2}$; $w^{-1} = \sigma^2(F_o^2) + (0.0279 \times F_o^2)^2$ for $UFeS_3$ at 80 K; $w^{-1} = \sigma^2(F_o^2) + (0.0269 \times F_o^2)^2$ for $UFeS_3$ at 100 and 297 K; $w^{-1} = \sigma^2(F_o^2) + (0.0256 \times F_o^2)^2$ for $UFeSe_3$.

Single-Crystal Magnetic Measurements. The direct current (dc) magnetic susceptibility measurements have been performed with a Quantum Design MPMS magnetometer. Because a large, 14.5 mg, high-purity single crystal of $UFeSe_3$ was available, see photographs of the crystal in Supporting Information, Figure S1a, an extensive investigation of its magnetic properties has been carried out. In contrast, because of the problems arising from the presence of any secondary phase, a very small single-phase 0.202 mg single crystal of $UFeS_3$ was less extensively studied.

A $UFeSe_3$ crystal, see Supporting Information, Figure S1a, with 2.8, 0.5, and 1.2 mm dimensions for the *a*-, *b*-, and *c*-axes, respectively, was mounted in two different orientations, see Supporting Information, Figure S1b, on a rotator to study the angular dependence of its susceptibility. First, the crystal was rotated about the *a*-axis to determine the magnetic axes in the *bc*-plane, initially at 4.26 K, and then in steps up to 240 K, see Supporting Information, Figure S2. This rotation led to a maximum in the susceptibility along the *b*-axis and a minimum along the *c*-axis, the axes that correspond to the magnetic easy and hard axes, respectively, at 4.26 K. Second, the crystal was rotated about this *c*-axis, see Supporting Information, Figure S1b, to determine the magnetic axes in the *ab*-plane at 4.26 K. This rotation, see Supporting Information, Figure S3, led to a maximum in the susceptibility along the *b*-axis and to a minimum in the susceptibility situated at 90° from the maximum, a minimum that defines the magnetic intermediate axis, the *a*-axis at 4.26 K.

Following the determination of the magnetic axes, the $UFeSe_3$ crystal was sequentially mounted on a quartz rod in the three orientations of the magnetic axes observed at 4.26 K, and the magnetic moment was measured, after zero field cooling to 2 K, upon warming to 300 K in an applied field of 0.1 T. In a separate study the temperature dependence of the contribution of the quartz rod and the glue to the moment was measured. The temperature dependencies of the molar magnetic susceptibility of $UFeSe_3$ and $UFeS_3$ were calculated by subtracting the contribution of the quartz rod and glue and diamagnetic corrections of -0.000117 and -0.000093 emu/mol, respectively. The magnetization in the three $UFeSe_3$ single crystal orientations was measured at 4.3 K in applied fields of 0 to 7 T.

A subsequent study of the magnetic susceptibility of a 22 mg powder sample of $UFeSe_3$ led to results in good agreement with the average of the results of the three orientations of the $UFeSe_3$ single crystal. However, some differences, resulting from crystallite reorientation, were observed at low temperature.

Iron-57 Mössbauer Spectroscopy. The Mössbauer spectra were measured between 4.2 and 295 K in a Janis Supervaritemp cryostat with a constant-acceleration spectrometer that utilized a rhodium matrix cobalt-57 source and was calibrated at 295 K with α-iron powder. The Mössbauer spectral absorbers contained 20 mg/cm^2 of $UFeS_3$ and 18 mg/cm^2 of $UFeSe_3$ powder mixed with boron nitride. The thickness of the absorbers is limited by the strong uranium absorption of the 14.4 keV γ-rays and, consequently, the quality of the low-temperature magnetic Mössbauer spectra is somewhat reduced by this limitation.

Single-Crystal Resistivity Measurements. The electrical resistivity of a single crystal of $UFeSe_3$ was measured along the *a*-axis between 2 and 300 K by using a standard four-probe alternating current (ac) method and a Quantum Design PPMS instrument. A 1.38 mm long single crystal of $UFeSe_3$ was attached with Dow 4929N silver paint to four leads constructed of 8 μm diameter graphite fibers which were connected to 15 μm diameter copper wire. Resistance measurements above 10^9 Ω were made with a HP 3456A digital voltmeter in a two-probe configuration.

Optical Measurements. Black $UFeS_3$ or $UFeSe_3$ crystals were manually selected and ground. The purity of each sample was subsequently confirmed by powder X-ray diffraction measurements. The UV−vis−NIR diffuse reflectance spectra were collected at 293 K from 200 to 2500 nm, that is, from 6.21 to 0.50 eV, by using a Shimadzu UV3101 spectrophotometer. The Kubelka−Munk function[22] was used to convert diffuse reflectance data to absorption spectra.

Infrared spectra were recorded from 400 to 4000 cm^{-1}, that is, from 0.05 to 0.50 eV, by using a Nicolet 6700 FT-IR spectrometer.

Results and Discussion

Syntheses. $UFeSe_3$ was first prepared accidentally through the reaction of U, FeSe, Sb, and NaCl/KCl at 1073 K; small crystals of $UFeSe_3$ were produced in low yield. A rational synthesis using U, Fe, and Se in a stoichiometric ratio and a CsCl flux led to an almost complete reaction in which large single crystals of $UFeSe_3$ suitable for physical measurements were obtained.

In a similar manner $UFeS_3$ was synthesized; however, U_2FeS_5 and other secondary phase binary compounds were also produced. Attempts to prepare pure $UFeS_3$ by using different starting materials, stoichiometries, and temperature regimes failed. Interestingly, by increasing the U/Fe ratio, U_2FeS_5 became the major product, and another ternary uranium iron sulfide,[23] U_8FeS_{17}, formed. The relative yields of $UFeS_3$, U_2FeS_5,[13] and U_8FeS_{17} can be varied by changing the U/Fe ratio. No iron(III) impurity was detected in the X-ray powder diffraction pattern of $UFeS_3$, but Mössbauer spectral measurements

(21) Ravel, B.; Newville, M. *J. Synchrotron Rad.* **2005**, *12*, 537–541.

(22) Kubelka, P.; Munk, F. *Z. Tech. Phys.* **1931**, *12*, 593–601.

(23) Kohlmann, H.; Stöwe, K.; Beck, H. P. *Z. Anorg. Allg. Chem.* **1997**, *623*, 897–900.

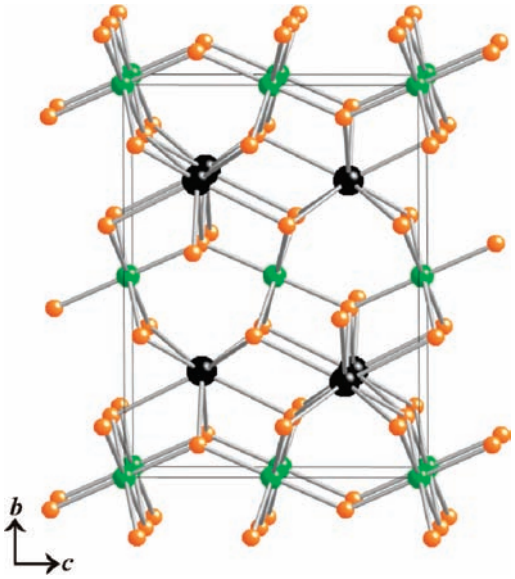

Figure 1. Crystal structure of $UFeS_3$ and $UFeSe_3$ along the *a*-axis. Here and in Figures 2 and 3 the color code is U, black; Fe, green; S or Se, orange.

reveal the presence of a trace of an unidentified iron(III) impurity. In contrast, $UFeSe_3$ was the only ternary uranium−iron selenide that could be found in the reactions of U/Fe/Se under the numerous conditions used.

Structures of $UFeS_3$ and $UFeSe_3$. The $UFeS_3$ and $UFeSe_3$ compounds are isostructural; their structures have been previously reported.[8,9] As is shown in Figure 1, the structure consists of alternating layers of US_8 or USe_8 bicapped trigonal prisms and layers of FeS_6 or $FeSe_6$ octahedra. Each of the bicapped trigonal prisms shares trigonal faces along the *a*-axis to form a single chain that is further edge-shared with two neighbors along the *c*-axis to form individual $^2_\infty[US_8]$ or $^2_\infty[USe_8]$ sheets (Figure 2a). Within the FeS_6 or $FeSe_6$ layers, each octahedron shares edges along the *a*-axis to form a single chain; each of these chains corner-shares with two identical chains along the *c*-axis (Figure 2b). Between the layers, US_8 or USe_8 and FeS_6 or $FeSe_6$ polyhedra further connect to each other by edge- and corner-sharing.

Selected interatomic distances for $UFeS_3$ and $UFeSe_3$ are listed in Table 2. The distances for $UFeS_3$ are within 0.01 Å of those reported earlier.[9] The U−S distances at 100 K are 2.755(1) to 2.977(1) Å. In $UFeSe_3$ the U−Se distances at 297 K are 2.886(1) to 3.117(1) Å. The Fe−S distances at 100 K are 2.3753(7) and 2.5517(8) Å. The Fe−Se distances are 2.4968(7) and 2.6782(7) Å. The shortest U−U/Fe-Fe distances, that is, the length of the *a*-axis, of 3.7905(1) Å in $UFeS_3$ at 100 K and of 3.9457(8) Å in $UFeSe_3$ at 297 K, are found within the layers. The shortest U−Fe distances between the layers are 3.5639(2) Å in $UFeS_3$ at 100 K and 3.7546(7) Å in $UFeSe_3$ at 297 K. A comparison of the 297 K $UFeS_3$ U−S and Fe−S interatomic distances with the $UFeSe_3$ U−Se and Fe−Se interatomic distances indicates that the latter interatomic distances are consistently longer by about 0.12 Å or about 4.5 %.

(24) Marezio, M.; Remeika, J. P.; Dernier, P. D. *Acta Crystallogr., Sect. B: Struct. Crystallogr. Cryst. Chem.* **1970**, *26*, 2008–2022.

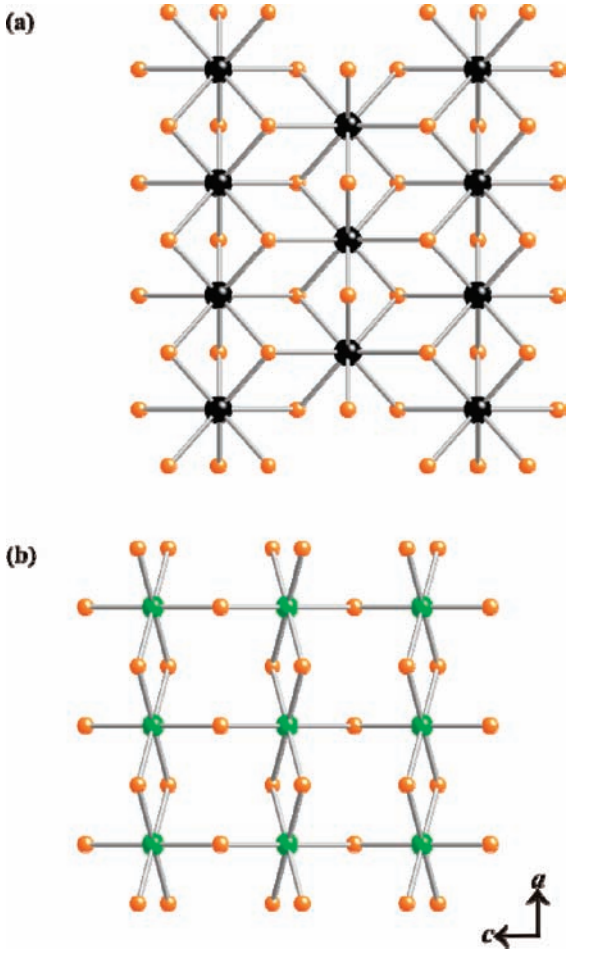

Figure 2. Individual US_8 or USe_8 layer (a) and FeS_6 or $FeSe_6$ layer (b) viewed down the *b*-axis.

Table 2. Selected Interatomic Distances (Å) for $UFeS_3$ and $UFeSe_3$

	$UFeS_3$, 80 K	$UFeS_3$, 100 K	$UFeS_3$, 297 K	$UFeSe_3$, 297 K
U−*Q*(1) × 4	2.7979(8)	2.7972(8)	2.8021(7)	2.9277(8)
U−*Q*(1) × 2	2.978(1)	2.977(1)	2.982(1)	3.117(1)
U−*Q*(2) × 2	2.756(1)	2.755(1)	2.761(1)	2.886(1)
Fe−*Q*(1) × 4	2.5514(8)	2.5517(8)	2.5633(7)	2.6782(7)
Fe−*Q*(2) × 2	2.3754(7)	2.3753(7)	2.3794(6)	2.4968(7)
U−U/Fe−Fe	3.7911(1)	3.7905(1)	3.8009(1)	3.9457(8)
U−Fe	3.5637(2)	3.5639(2)	3.5783(2)	3.7546(7)

The $AnMQ_3$ compounds adopt two basic structure types, namely, that of $UFeS_3$[1] (Figure 1) or $GdFeO_3$.[24] When *M* = Sc, Fe, or Mn the $UFeS_3$ structure type is adopted; when *M* = V, Cr, Co, Ni, Ru, or Rh then the $GdFeO_3$ structure type is adopted. The coordination environments for the metals are very similar in these structures, but the connectivities between the metal polyhedra are different. In the $GdFeO_3$-structure type[24] (Figure 3) the MQ_6 octahedra share corners only with each other in the *ac*-plane. However, they are further connected along the *b*-axis via corner sharing to form three-dimensional channels filled with bicapped trigonal prismatic *An* polyhedra. The reason why the various $AnMQ_3$ compounds adopt one or the other structure is not clear. The relative sizes of the metals may be partially responsible for the difference, but there is no clear trend. Among the lanthanide compounds, $LaYbS_3$ can form

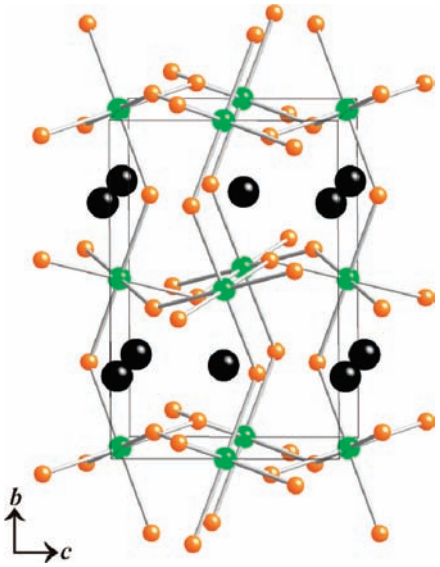

Figure 3. Unit cell of the $GdFeO_3$ structure type adopted by $AnMQ_3$ where M may be V, Cr, Co, Ni, Ru, or Rh.

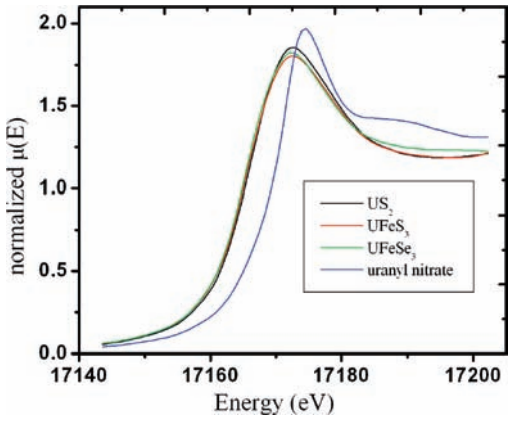

Figure 4. X-ray absorption near edge spectra of $UFeS_3$, $UFeSe_3$, US_2, and uranyl nitrate measured, at the uranium L_3-edge at room temperature.

either structure type under different reaction temperatures.[25] The size of the chalcogens could also play a role because $GdScS_3$ is isostructural with $UFeS_3$, whereas $GdScSe_3$ is isostructural with $GdFeO_3$. However, similar behavior has not been observed in related actinide transition-metal chalcogenides.[26]

X-ray Absorption Spectroscopy. The X-ray absorption near-edge spectra of $UFeS_3$ and $UFeSe_3$, as well as that of the uranium(IV) standard, US_2, are shown in Figure 4; the spectrum of uranyl nitrate is also shown for comparison. This figure reveals that the shapes and the positions of the edges of $UFeS_3$, $UFeSe_3$, and US_2 are all similar. Hence uranium is tetravalent, as expected; this means that $UFeS_3$ and $UFeSe_3$ contain iron(II). This is confirmed by the iron-57 Mössbauer spectral results presented below.

Single-Crystal Magnetic Measurements. The temperature dependencies of the molar magnetic susceptibility, χ_M, of single crystals of $UFeSe_3$ and $UFeS_3$, measured along three and two directions, after zero-field cooling to 2 K and subsequent warming to 300 K in a 0.1 T applied field, are shown in Figures 5 and 6, respectively. A broad maximum in χ_M is observed when the field is applied parallel to the a-axis at about 53 K for $UFeSe_3$ and about 70 K for $UFeS_3$. Because of the limited amount of data obtained on a very small single crystal of $UFeS_3$, the discussion of the magnetic properties will be restricted to those of $UFeSe_3$.

A strong magnetic anisotropy is observed in $UFeSe_3$ as is illustrated in Figure 5. The molar magnetic susceptibilities measured along the b- and c-axes exhibit temperature dependencies that are very different and different from that measured parallel to the a-axis. The value of χ_M along the b-axis increases continuously with decreasing temperature and at 107 K exhibits a small shoulder-like feature that is expanded in the upper inset and a change of slope below 10 K as is shown in the lower inset to Figure 5. All the small features shown in the insets have been reproduced in a second single crystal and a powder study of the magnetic susceptibility of $UFeSe_3$. In contrast, the value of χ_M measured along the c-axis exhibits a small increase as the sample was cooled from 300 to about 140 K and is, upon further cooling to 2 K, virtually constant at about 0.009 emu/mol, a temperature independent susceptibility that is similar to that observed[27] in both URuAl and UFe_2Si_2. From 2 to 40 K the magnetic anisotropy favors the b-axis, whereas, above 40 K, it favors the a-axis.

The occurrence of strong magnetic anisotropy in uranium(IV) containing compounds is well documented,[27,28] for instance, in UCl_4 and various intermetallic compounds, and a systematic trend in the orientation of the magnetic anisotropy in uranium(IV) compounds has been delineated.[27] If the uranium(IV) near neighbors are within a plane, their moments preferentially align perpendicular to the plane and axial magnetic anisotropy is observed. In contrast, if the uranium(IV) near neighbors form a chain, their moments preferentially align in a plane perpendicular to the chain axis, and planar magnetic anisotropy is observed.

In $UFeSe_3$ and $UFeS_3$ the uranium(IV) ions are arranged in the ac-plane, and the shortest U−U distance is observed along the a-axis, see Figure 2. Hence, if the uranium arrangement is described as planar, the easy-axis is expected along the b-axis as is observed below 40 K and if the uranium arrangement is described as axial, the

(25) Rodier, N.; Julien, R.; Tien, V. *Acta Crystallogr., Sect. C: Cryst. Struct. Commun.* **1983**, *39*, 670–673.
(26) Jin, G. B.; Choi, E. S.; Albrecht-Schmitt, T. E. *J. Solid State Chem.* **2009**, *182*, 1075–1081.

(27) (a) Sechovsky, V.; Havela, L. In *Handbook of Magnetic Materials*; Buschow, K. H. J., Ed.; Elsevier: Amsterdam, The Netherlands, 1998; Vol. *11*, p 1. (b) Sechovsky, V.; Havela, L. In *Handbook of Magnetic Materials*; Wohlfarth, E. P., Buschow, K. H. J., Eds.; Elsevier: Amsterdam, The Netherlands, 1988; Vol. *4*, Chapter 4, pp 309−491. (c) Arko, A. J.; Joyce, J. J.; Havela, L. In *The Chemistry of the Actinides and Transactinide Elements*, 3rd ed.; Morss, L. R., Edelstein, N. M., Fuger, J., Eds.; Springer: Berlin, 2006; Vol *4*, Chapter 21, pp 2307−2379. (d) Veenhuizen, P. A.; de Boer, F. R.; Menovsky, A. A.; Sechovsky, V.; Havela, L. *J. Phys.*(*Paris*) **1988**, *49*(C8), 485. (e) Sechovsky, V.; Havela, L.; de Boer, F. R.; Veenhuizen, P. A.; Sugiyama, K.; Kuroda, T.; Sugiura, E.; Ono, M.; Date, M.; Yamagishi, A. *Physica B* **1992b**, *177*, 164. (f) Sechovsky, V.; Havela, L.; Nakotte, H.; de Boer, F. R.; Brück, E. *J. Alloys Compd.* **1994**, *207*−*208*, 221. (g) de Boer, F. R.; Brück, E.; Menovsky, A. A.; Veenhuizen, P. A.; Sechovsky, V.; Havela, L.; Buschow, K. H. J. *Physica B* **1989**, *155*, 231.
(28) Edelstein, N. M.; Lander, G. H. In *The Chemistry of the Actinide and Transuranium Elements*; Morss, L. R., Edelstein, N. M., Fuger, J., Eds.; Springer: Dordrecht, The Netherlands, 2006; Vol. *4*, p 2225; Gamp, E.; Edelstein, N. M.; Khan Malek, C.; Hubert, S.; Genet, M. *J. Chem. Phys.* 1983, *79*, 2023.

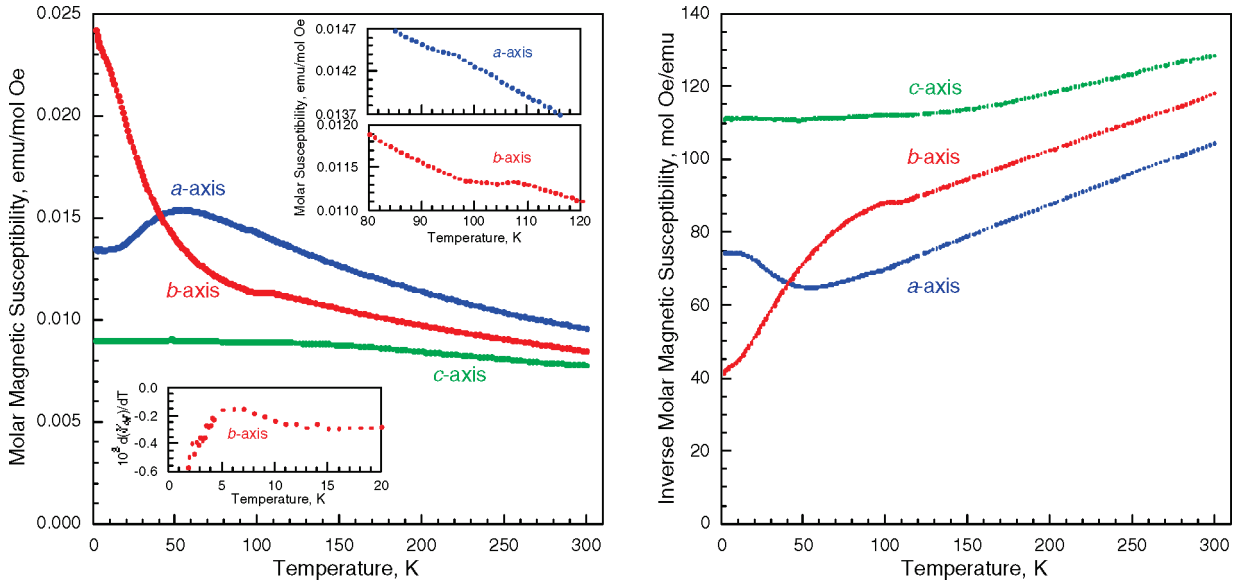

Figure 5. Molar magnetic susceptibility, left, and its inverse, right, obtained on a 14.5 mg single crystal of $UFeSe_3$ measured, after zero-field cooling, in a 0.1 T field applied parallel to the *a*-axis, blue, the *b*-axis, red, and the *c*-axis, green. The upper inset shows the expanded χ_M along the *a*- and *b*-axes, and the lower inset shows the derivative of χ_M in units of emu/mol Oe K measured at lower temperatures along the *b*-axis.

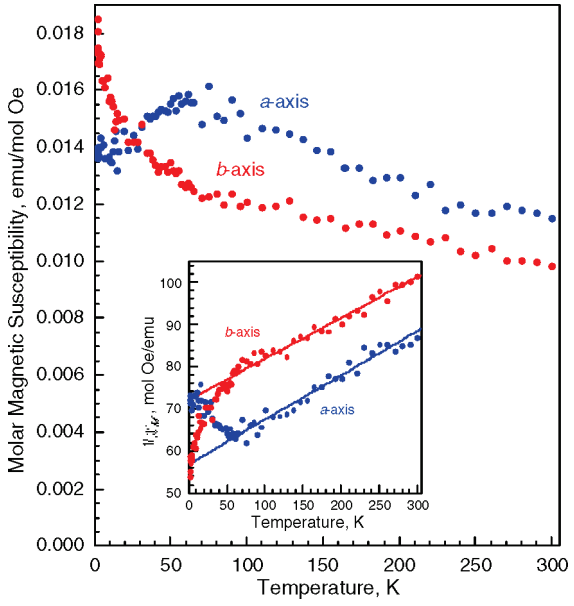

Figure 6. Molar magnetic susceptibility and its inverse, inset, obtained on a 0.20 mg single crystal of $UFeS_3$ measured, after zero-field cooling, in a 0.1 T field applied parallel to the *a*-axis, blue, and the *b*-axis, red. In the inset the lines correspond to a fit of $1/\chi_M$ between 110 and 300 K.

easy-axis is expected in the *bc*-plane in agreement with the observed *b*-axis below 40 K. As a result, the uranium(IV) magnetic anisotropy cannot be responsible for the easy *a*-axis anisotropy observed above 40 K, an anisotropy that is thus assigned to the iron(II) single ion anisotropy. In conclusion, the magnetic anisotropy is dominated by iron(II) and uranium(IV) above and below 40 K, respectively.

Although the magnetic anisotropy exhibited by $UFeSe_3$ is not unexpected, the temperature dependencies of χ_M measured along three directions (see Figure 5) and, more specifically the magnitude of the observed changes, are rather puzzling. None of the directions exhibits the large increase or decrease in the susceptibility that would indicate cooperative long-range ferromagnetic or antiferromagnetic ordering, that is, the observed χ_M in all directions is always rather small and continuously varies with temperature. However, along the *a*-axis, χ_M exhibits a broad maximum at about 50 K and is essentially constant below 12 K at about 0.0134 emu/mol Oe. Similar changes have been reported[27] in uranium(IV) compounds and assigned either to the temperature dependent population of the crystal field split J_z levels in lower than octahedral symmetry or to the spin fluctuations.

The field dependence of the 4.3 K molar magnetization of $UFeSe_3$ measured along the three axes is shown in Figure 7; a similar plot along two axes for $UFeS_3$ is shown in the Supporting Information, Figure S4. The magnetization along the *a*- and *c*-axes increases linearly with the applied field up to 7 T, whereas the magnetization along the *b*-axis increases linearly to about 2 T and continues to increase with a decreasing slope above 2 T. As expected, the slope of the magnetization between 0 and 7 T along the *a*-axis and the *c*-axis and between 0 and 2 T along the *b*-axis agrees well with the 4.3 K χ_M shown in Figure 5. An identical result was obtained at 2 K along the *a*-axis of a second single crystal. A linear behavior of the magnetization was observed[31] in $UCrS_3$ in an applied field of as much as 14 T in spite of the presence of a small "ferromagnetic" moment. This linear behavior indicates[31] that the domain walls do not move below a threshold field because of the presence of a large magnetocrystalline anisotropy with an energy comparable to the magnetic exchange energy.

Because the field and temperature dependencies of the magnetization and χ_M exhibit no indication of long-range magnetic ordering, the temperature dependence of $1/\chi_M$ of $UFeSe_3$ has been fit with the Curie−Weiss law, under

(29) Noël, H. *J. Less-Common Met.* **1986**, *121*, 265–270.
(30) Wertheim, G. K.; Guggenheim, H. J.; Levinstein, H. J.; Buchanan, D. N. E.; Sherwood, R. C. *Phys. Rev.* **1968**, *173*, 614–616.
(31) Wolfers, P.; Fillion, G.; Bacmann, M.; Noël, H. *J. Phys.* (*Paris*) **1976**, *37*, 233–239.

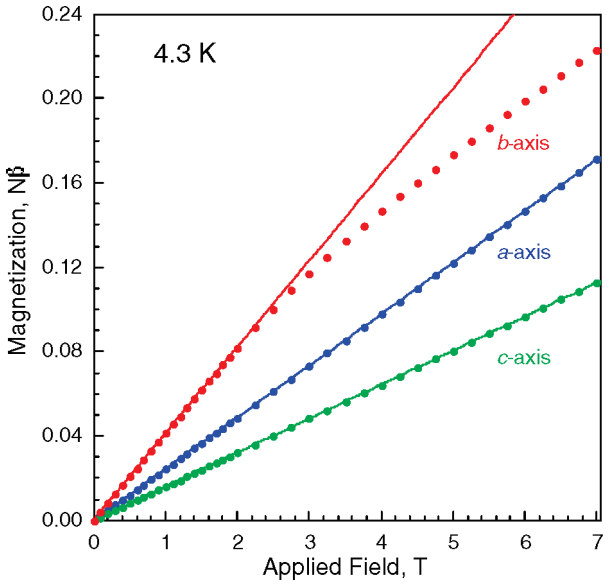

Figure 7. Magnetization of $UFeSe_3$ obtained at 4.3 K with the field applied along the *a*-axis, blue, the *b*-axis, red, and the *c*-axis, green. The linear fit for the *b*-axis includes only the 0 to 2 T magnetization.

the assumption that the mean-field model is a valid approximation for this compound. Fits of $1/\chi_M$ above 100, 100, and 120 K with the field parallel to the *a*-, *b*-, and *c*-axis, respectively, yield Curie constants of 5.78, 6.44, and 11.56 emu/mol Oe and corresponding μ_{eff} values of 6.80, 7.18, and 9.61 μ_B, respectively. The moments of 6.80 and 7.18 μ_B are within the range of 6.1 to 7.6 μ_B per mol expected, first, for a spin-only high-spin iron(II) ion with $S = 2$ and $g = 2$ and a uranium(IV) ion with $J = 4$ and $g_J = 0.8$ and, second, for a high-spin iron(II) ion with $S = 2$, $L = 2$, $J = 4$, and $g_J = 1.5$ and a uranium(IV) ion with $J = 4$ and $g_J = 0.8$. The effective moment of 9.61 μ_B is too large and indicates the inadequacy of the mean-field model in describing the magnetic properties along the *c*-axis. The corresponding Weiss temperatures are −306, −470, and −1177 K along the *a*-, *b*-, and *c*-axis, respectively, large negative Weiss temperatures that also indicate the inadequacy of the mean-field model. An estimate of the paramagnetic anisotropy can be obtained[27a,b] from the absolute difference between the Curie−Weiss temperatures along the *a*- and *c*- axes and the *b*- and *c*- axes. The differences of 871 and 707 K observed herein indicate a strong anisotropy between the *a*- and *b*-axes and the *c*-axis, that is, the low temperature anisotropy persists above about 110 K. In spite of the limitations of the mean-field model, the values of χ_M observed along the *a*- and *b*-axes for $UFeSe_3$ above about 110 K are consistent with the presence of independent paramagnetic high-spin iron(II) and uranium(IV) ions.

A close inspection of the molar magnetic susceptibility of $UFeSe_3$ reveals an additional, weak "shoulder-like" feature, at 107 K when the field is applied parallel to the *b*-axis and at 96 K when the field is applied parallel to the *a*-axis, see the upper insets to Figure 5. The 107 K temperature at which this shoulder appears corresponds to the observation of a magnetic hyperfine field in the iron-57 Mössbauer spectra of $UFeSe_3$, (see below). Thus, this feature could be associated with either long-range or short-range ordering and/or correlation of the iron(II) and/or uranium(IV) magnetic moments. However, because there is no indication of any long-range magnetic ordering in the temperature and field dependence of the magnetic properties of $UFeSe_3$, this feature must be associated with either short-range magnetic correlations or the onset of slower spin fluctuations.

The anisotropic magnetic behavior of $UFeS_3$ and $UFeSe_3$ at low temperatures is very similar to that observed in other two-dimensional antiferromagnetic uranium-containing or iron-containing compounds. Some examples are US_3, USe_3,[29] and Rb_2FeF_4,[30] in which the magnetic interactions are confined to the UQ_8 or FeF_6 polyhedral layers. In a fashion similar to that observed in $UFeS_3$ and $UFeSe_3$, the UQ_8 layers in the UQ_3 compounds are constructed with single chains of face-sharing UQ_8 bicapped trigonal prisms. The susceptibilities of US_3 and USe_3 exhibit antiferromagnetic ordering at 50 and 45 K, respectively, in a field applied parallel to the chain direction; more diffuse maxima are observed in a field applied perpendicular to the chain direction. In an analogous fashion, in Rb_2FeF_4 each FeF_6 octahedron corner shares within the *ab* plane to form tetragonal layers separated by Rb^+ cations along the *c*-axis. Magnetic susceptibility studies indicate that the iron(II) moments in Rb_2FeF_4 are perpendicular to the *c*-axis and that the susceptibility along the *a*-axis shows a broad maximum at 90 K. The susceptibility never reaches zero at 0 K along any axis and decreases slowly above 90 K. As has already been suggested,[29] this magnetic behavior is most likely the result of anisotropic two-dimensional magnetic interactions between the metal cations. However, for $UFeS_3$ and $UFeSe_3$ the magnetic structure is more complex than for UQ_3 and Rb_2FeF_4, as there are two different layers with two different magnetic cations and there may be magnetic interactions between the layers through the sulfur or selenium anions.

In contrast to $UFeS_3$ and $UFeSe_3$, the isostructural $UMnSe_3$[4] and $ThMnTe_3$[2] compounds are both ferromagnetic with a T_C of 70 and 62 K, respectively. Clearly the magnetic interactions involving transition metals have a major impact on the overall magnetic behavior of the compounds. A less dramatic influence of the 3d transition metals has been observed in U_8MQ_{17}, where *M* is a 3d transition-metal cation and *Q* is S or Se, compounds in which the weight percent of *M* is much reduced.[11] In these compounds the *M*−U exchange interactions are believed[11] to play a crucial role in the onset of the magnetic ordering. In $UCrS_3$[31] and U_2FeS_5[10] the coordination environments about the *M* cations and the U−U distances are similar to those observed in $UFeS_3$ and $UFeSe_3$, and neutron diffraction studies[10] have shown that the 3d transition-metal cation moments are antiferromagnetically aligned and the uranium moments are canted in the former compounds. All these earlier observations suggest that both the iron(II) and the uranium(IV) moments participate in the magnetic ordering of $UFeS_3$ and $UFeSe_3$, an ordering that may be complex. A possible description of the magnetic behavior of $UFeS_3$ and $UFeSe_3$ based upon both the magnetic, electric, and Mössbauer spectral measurements is proposed below.

Iron-57 Mössbauer Spectroscopy. Selected Mössbauer spectra for $UFeS_3$ and $UFeSe_3$ are shown in Figures 8 and 9, respectively. It is immediately obvious from these

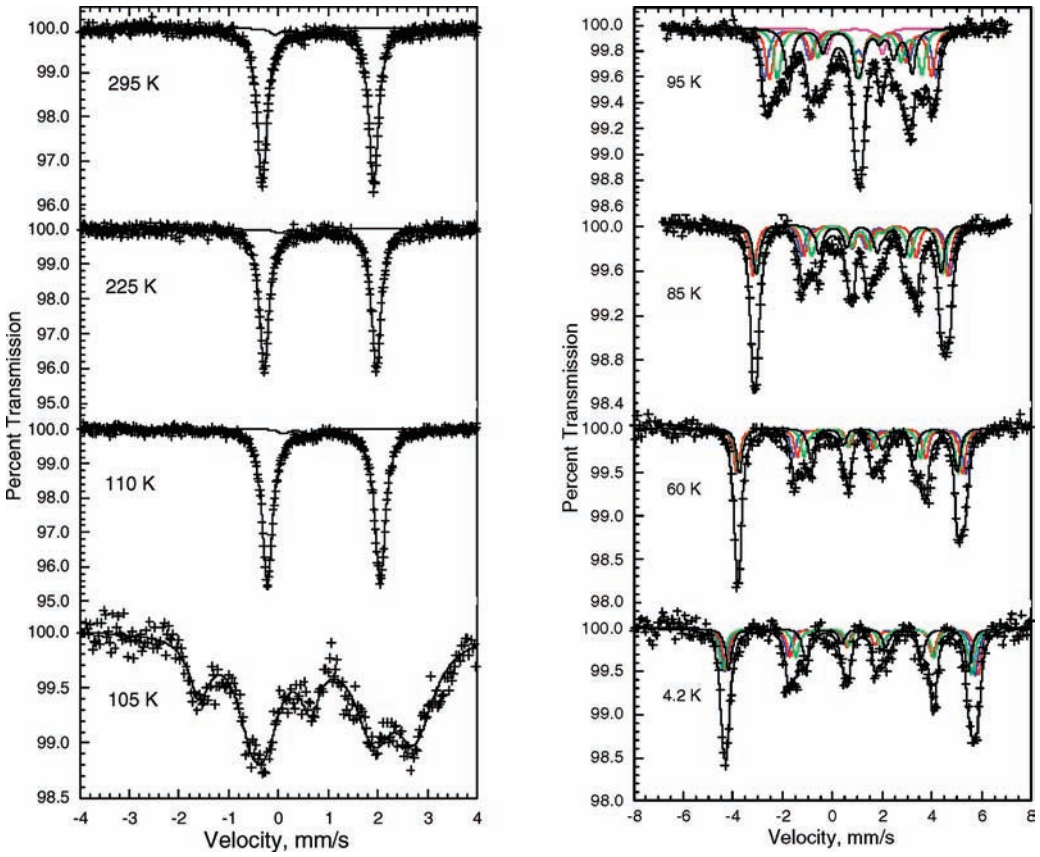

Figure 8. Iron-57 Mössbauer spectra of $UFeS_3$ obtained at the indicated temperatures.

figures that the iron-57 nuclei experience a static hyperfine field on the Larmor precession time of about 0.05 μs below 110 K. This magnetic behavior is no doubt associated with the shoulder observed in the magnetic susceptibility of $UFeSe_3$ at 96 or 107 K in an applied field parallel to the *a*- or *b*-axis, respectively. Such Mössbauer spectra may result[30] from short- or long-range magnetic ordering of the iron magnetic moments or from an increase in the spin-fluctuation time of short-range magnetic ordering below 110 K.

The paramagnetic spectra of $UFeS_3$ and $UFeSe_3$ obtained at and above 110 K have been fit with one symmetric Lorentzian quadrupole doublet, whose spectral parameters are given in Tables 3 and 4, respectively. In addition to the main doublet in the spectra of $UFeS_3$ there is a minor doublet, whose area represents 3% of the total absorption area, a doublet that may be assigned to an iron(III) impurity.

The magnetic spectra of $UFeS_3$ and $UFeSe_3$, obtained between 4.2 and 105 K, have been fit with four magnetic components with identical line widths, isomer shifts, quadrupole interactions, $e^2Qq/2$, and asymmetry parameters, η, but with different hyperfine fields, and Euler angles, θ and ϕ, between the principal axis of the electric field gradient tensor and the hyperfine field. The simultaneous presence of a relatively narrow line at about -4.4 mm/s in $UFeS_3$ at 4.2 K and at about -3.4 mm/s in $UFeSe_3$ at 10 K and of a rather broad line at $+5.9$ mm/s in $UFeS_3$ at 4.2 K and at about $+4.9$ mm/s in $UFeSe_3$ at 10 K rules out fitting the spectra with a single magnetic sextet; fits with fewer than four components were unsuccessful. Fits with additional components did not improve the χ^2 values, values that are close to one for all the fits shown in Figures 8 and 9.

The temperature dependencies of the isomer shift in $UFeS_3$ and $UFeSe_3$ are shown at the top of Figure 10. Isomer shift values between 0.94 and 0.80 mm/s are characteristic[32] of high-spin iron(II) octahedrally coordinated to sulfur or selenium. Hence, both the iron-57 Mössbauer spectra and uranium L_3-edge X-ray absorption spectra indicate, without question, that uranium is tetravalent and iron is divalent in both $UFeS_3$ and $UFeSe_3$. The high-spin iron(II) isomer shift increases[33] with iron coordination number. For high-spin iron(II) tetrahedrally coordinated to sulfur,[33] 4.2 K isomer shifts of 0.65 mm/s are usual, and larger isomer shifts of about 0.8 mm/s have been observed[32] for high-spin iron(II) with for 5-fold coordination. Hence, the low temperature isomer shifts of 0.92 to 0.94 mm/s observed herein are normal for high-spin iron(II) octahedrally coordinated to sulfur. Their temperature dependencies have been fit with the Debye model[34] for a solid, and the resulting Mössbauer temperatures, Θ_M, are $3.4(4) \times 10^2$ and $2.9(3) \times 10^2$ K for $UFeS_3$ and $UFeSe_3$, respectively.

The temperature dependence of the logarithm of the spectral absorption area in $UFeS_3$ and $UFeSe_3$ is shown

(32) Osterloh, F.; Saak, W.; Pohl, S.; Kroeckel, M.; Meier, C.; Trautwein, A. X. *Inorg. Chem.* **1998**, *37*, 3581–3587.
(33) Hoggins, J. T.; Steinfink, H. *Inorg. Chem.* **1976**, *15*, 1682–1685.
(34) Shenoy, G. K.; Wagner, F. E.; Kalvius, G. M. In *Mössbauer Isomer Shifts*; Shenoy, G. K., Wagner, F. E., Eds.; North-Holland Publishing Company: The Netherlands, 1978; p 51.

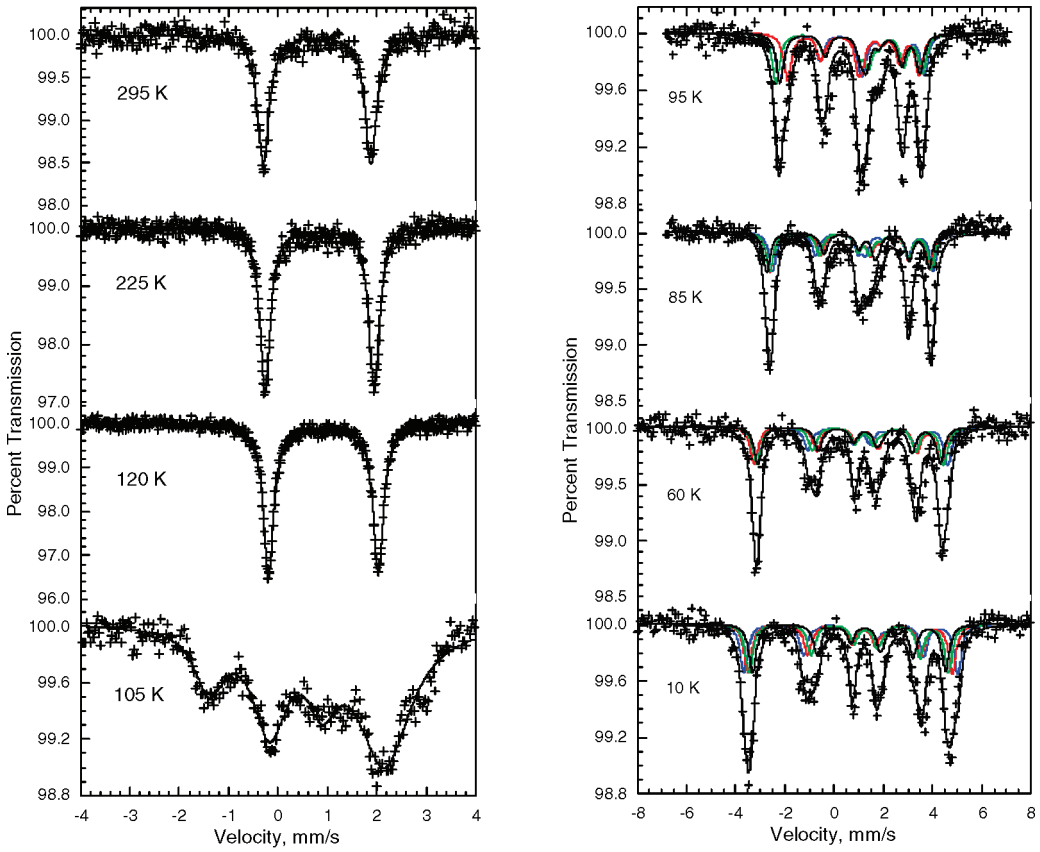

Figure 9. Iron-57 Mössbauer spectra of $UFeSe_3$ obtained at the indicated temperatures.

Table 3. Mössbauer Spectral Parameters of $UFeS_3$

T, K	δ,[a] mm/s	ΔE_Q,[b] mm/s	H_{ave}, T	Γ,[c] mm/s	area, (%ε) (mm/s)
295	0.793(5)	−2.245(5)	0	0.231(5)	2.81(1)
225	0.841(5)	−2.256(5)	0	0.230(5)	3.14(1)
155	0.889(5)	−2.255(5)	0	0.234(5)	3.54(1)
120	0.909(5)	−2.252(5)	0	0.233(5)	3.65(1)
110	0.912(5)	−2.267(5)	0	0.252(5)	3.84(1)
102	0.860(5)	−2.25(1)	9.93(1)	0.35(1)	3.98(1)
95	0.885(5)	−2.25(1)	15.30(1)	0.35(1)	3.98(1)
85	0.909(5)	−2.29(1)	20.73(1)	0.33(1)	4.09(1)
60	0.925(5)	−2.30(1)	25.20(1)	0.30(1)	4.15(1)
30	0.921(5)	−2.30(1)	27.83(1)	0.30(1)	4.25(1)
4.2	0.946(5)	−2.30(1)	28.58(1)	0.31(1)	4.34(1)

[a] The isomer shifts are given relative to α-iron powder at 295 K. [b] ΔE_Q is the paramagnetic quadrupole splitting, $(e^2Qq/2)(1 + \eta^2/3)^{1/2}$, with $\eta = 1$. [c] Full line width at half-height.

Table 4. Mössbauer Spectral Parameters of $UFeSe_3$

T, K	δ,[a] mm/s	ΔE_Q,[b] mm/s	H_{ave}, T	Γ,[c] mm/s	area, (%ε) (mm/s)
295	0.790(5)	−2.176(5)	0	0.282(5)	2.08(1)
225	0.841(5)	−2.208(5)	0	0.255(5)	2.43(1)
155	0.892(5)	−2.222(5)	0	0.263(5)	2.83(1)
120	0.918(5)	−2.221(5)	0	0.257(5)	2.97(1)
110	0.918(5)	−2.223(5)	0	0.286(5)	3.10(1)
105	0.928(5)	−2.222(10)	5.58(1)	0.32(1)	3.26(1)
95	0.923(5)	−2.223(10)	14.17(1)	0.37(1)	3.36(1)
85	0.935(5)	−2.225(10)	17.15(1)	0.34(1)	3.27(1)
60	0.936(5)	−2.230(10)	20.83(1)	0.39(1)	3.60(1)
30	0.939(5)	−2.230(10)	22.81(1)	0.39(1)	3.58(1)
10	0.937(5)	−2.230(10)	22.95(1)	0.37(1)	3.44(1)

[a] The isomer shifts are given relative to α-iron powder at 295 K. [b] ΔE_Q is the paramagnetic quadrupole splitting, $(e^2Qq/2)(1 + \eta^2/3)^{1/2}$, with $\eta = 1$. [c] Full line width at half-height.

at the bottom of Figure 10 and has been fit with the Debye model[34] for a solid. The resulting Debye temperatures, Θ_D, are 269(5) and 243(7) K for $UFeS_3$ and $UFeSe_3$, respectively. The Debye and Mössbauer temperatures are not directly related, because the temperature dependence of the isomer shift probes[34] more specifically the high-energy phonons and the Mössbauer temperature, Θ_M, is usually observed to be higher than the Debye temperature, Θ_D. The ratio of about 1.5 observed herein is similar to that observed[35] for intermetallics and is smaller than those typically observed[36−40] for organometallic compounds.

Magnetic Mössbauer Spectra. The four components used in the Mössbauer spectral fits for $UFeS_3$ and $UFeSe_3$ are unexpected on the basis of the single iron crystallographic site. However, the observation[41] of magnetically inequivalent sites for a unique crystallographic iron

(35) Drake, B. L.; Grandjean, F.; Kangas, M. J.; Okudzeto, E. K.; Karki, A. B.; Sougrati, M. T.; Young, D. P.; Long, G. J.; Chan, J. Y. *Inorg. Chem.* **2010**, *94*, 1852–1866.
(36) Reger, D. L.; Elgin, J. D.; Smith, M. D.; Grandjean, F.; Rebbouh, L.; Long, G. J. *Polyhedron* **2006**, *25*, 2616–2622.
(37) Reger, D. L.; Gardinier, J. R.; Gemmill, W. R.; Smith, M. D.; Shahin, A. M.; Long, G. J.; Rebbouh, L.; Grandjean, F. *J. Am. Chem. Soc.* **2005**, *127*, 2303–2316.
(38) Reger, D. L.; Gardinier, J. R.; Smith, M. D.; Shahin, A. M.; Long, G. J.; Rebbouh, L.; Grandjean, F. *Inorg. Chem.* **2005**, *44*, 1852–1866.
(39) Jiao, J.; Long, G. J.; Rebbouh, L.; Grandjean, F.; Beatty, A. M.; Fehlner, T. P. *J. Am. Chem. Soc.* **2005**, *127*, 17819–17831.
(40) Owen, T.; Grandjean, F.; Long, G. J.; Domasevitch, K. V.; Gerasimchuk, N. *Inorg. Chem.* **2008**, *47*, 8704–8713.

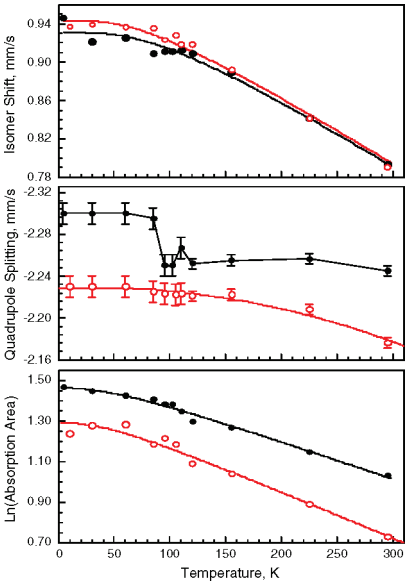

Figure 10. Temperature dependence of the isomer shift, top, the quadrupole splitting, center, and the logarithm of the absorption area, bottom, in $UFeS_3$, black solid points, and $UFeSe_3$, red open points. The solid lines in the top and bottom plots are the result of a fit with the Debye model for a solid. The red solid line in the center plot is the result of the fit discussed in the text.

site is common in Mössbauer spectra. The possibility of four magnetically inequivalent iron sites for $UFeS_3$ and $UFeSe_3$ and different hypotheses for the orientation of the hyperfine field in the electric field gradient tensor axes have been considered and are discussed in the Supporting Information. No simple collinear arrangement of the iron(II) magnetic moments and hence hyperfine fields could be found. If the small anomaly in the magnetic susceptibility at about 100 K is related to a long-range magnetic ordering, then the iron(II) magnetic moments may be non-collinear; a proposal that can only be verified by neutron diffraction measurements.

The temperature dependence of the average hyperfine field in $UFeS_3$ is shown in the inset to Figure 11; the temperature dependence for $UFeSe_3$ is similar. The average 4.2 K hyperfine field of 29 T is characteristic of high-spin iron(II). The effective magnetic hyperfine field, H_{eff}, at the iron nucleus results from the addition of three contributions,[42−44] H_{core}, the core field from the Fermi contact term, typically −44 T for high-spin iron(II), and H_{dip} and H_{orb}, the fields produced by the dipolar interaction of the nuclear magnetic moment with the electronic and orbital spin moment, respectively. Usually the latter two terms are rather small and opposite in sign to the core field. Hence, they reduce the absolute value of the observed effective magnetic hyperfine field.

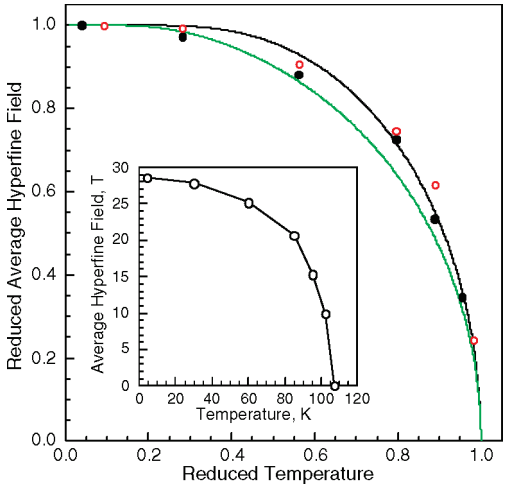

Figure 11. Reduced plot of the average hyperfine field in $UFeS_3$, black solid points, and $UFeSe_3$, red open points. The average 4.2 K hyperfine field and a critical temperature of 107 K have been used to obtain the reduced hyperfine field and temperature. The black and green solid lines are the Brillouin curves for $S = 1/2$ and 2, respectively. Inset: The temperature dependence of the average hyperfine fields observed in $UFeS_3$.

A reduced plot, H/H_0 versus T/T_c, of the average hyperfine field in $UFeS_3$ and $UFeSe_3$ is shown in Figure 11, where H_0 is the 4.2 K average hyperfine field and T_c is 107 K. Because the iron ions are high-spin iron(II), the reduced hyperfine field is expected to follow a Brillouin curve for $S = 2$, a curve that is shown as a green solid line in Figure 11. In reality, the reduced field follows a curve that is bracketed by the Brillouin curves for $S = 1/2$ and 2. This smooth Brillouin-like temperature dependence of the hyperfine field is indicative[30] of long-range magnetic order of at least the iron(II) magnetic moments. However, the requirement of at least four sextets to fit the spectra indicates that the magnetic order may be complex and can only be elucidated through single-crystal magnetic neutron diffraction measurements. Further, the change in magnetic anisotropy at about 40 K does not influence the line-shape profile of the Mössbauer spectra.

All the fits of the magnetic Mössbauer spectra of $UFeS_3$ and $UFeSe_3$ required an asymmetry parameter, η, of 1, the maximum possible value for this parameter. This large value is required to fit the line shape observed at about −1 and +2.5 mm/s in $UFeS_3$ and at about −0.6 and +2 mm/s in $UFeSe_3$. A value of $\eta = 1$ indicates that the principal axis of the electric field gradient tensor at the iron(II) site has less than 4-fold symmetry, in agreement with the $2/m$ site symmetry.

The magnetic spectra are only compatible with a negative quadrupole interaction, and the temperature dependence of the quadrupole splitting, $\Delta E_Q = (e^2Qq/2)(1 + \eta^2/3)^{1/2}$, for $UFeS_3$ and $UFeSe_3$ is shown in the center of Figure 10. The fits of the magnetic spectra are not very sensitive to the value of ΔE_Q because it and the other hyperfine parameters, and especially ΔE_Q and the θ angle, are highly correlated. As a result, ΔE_Q was fixed at values that were reasonable in view of the paramagnetic quadrupole splittings, and the χ^2 values were monitored to remain within the error bars shown in the center of Figure 10. It is clear that for $UFeS_3$, fits with a ΔE_Q of about −2.25 mm/s at 4.2, 30, 60, and 85 K would be significantly poorer than the best fits obtained herein.

(41) Long, G. J.; Hermann, R. P.; Grandjean, F.; Chacon, C.; Isnard, O. *J. Phys.: Condens. Matter* **2006**, *18*, 10765–10773. Grandjean, F.; Hermann, R. P.; Popiel, E.; Long, G. J. *J. Appl. Phys.* **2007**, *101*, 023917/1−6.
(42) Cranshaw, T. E.; Longworth, G. In *Mössbauer Spectroscopy Applied to Inorganic Chemistry*; Long, G. J., Ed.; Plenum: New York, 1984; Vol. *1*, p 171.
(43) Thomas, M. F.; Johnson, C. E. In *Mössbauer Spectroscopy*; Dickson, D. P. E., Berry, F. J., Eds.; Cambridge University Press: Cambridge, U.K., 1986; p 143.
(44) Carling, S. G.; Hautot, D.; Watts, I. D.; Day, P.; Visser, D.; Ensling, J.; Gütlich, P.; Long, G. J.; Grandjean, F. *Phys. Rev. B* **2002**, *66*, 104407 (12 p.).

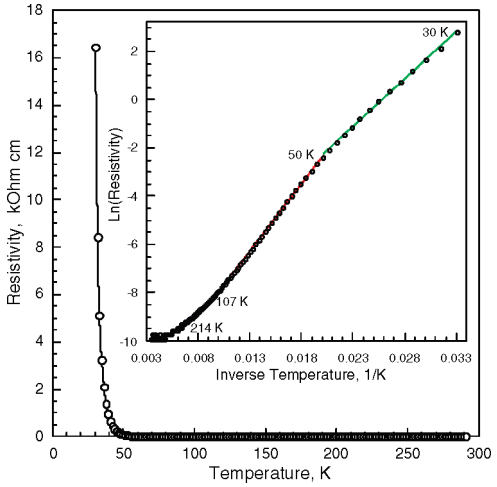

Figure 12. Temperature dependence of the electrical resistivity of a single crystal of $UFeSe_3$ obtained with the current parallel with the *a*-axis. Inset: An Arrhenius plot of ln ρ versus $1/T$ with a linear fit between 30 and 50 K, the green line, 50 and 107 K, the red line, and 107 and 214 K, the blue line; a blue line that may be difficult to see.

Hence, there is a real change in ΔE_Q between 85 and 100 K, that is, at or just below the temperature of the shoulder-like feature in the magnetic susceptibility measured along the *a*- and *b*-axes. This change in ΔE_Q is likely to result[30] from some magnetostriction. The temperature dependence of ΔE_Q for $UFeSe_3$ is also shown in the center of Figure 10. Any change in ΔE_Q around 107 K is less obvious than it is in $UFeS_3$, but may be present. A fit with the Ingalls[45] model for the temperature dependence of ΔE_Q for $UFeSe_3$ is poor, predominately because of the very small change in ΔE_Q observed between 4.2 and 295 K. This occurs because the low-symmetry component of the pseudo-octahedral crystal field is sufficient to remove the degeneracy of the iron(II) t_{2g} orbitals to an extent that there is no change in their occupancy between 4.2 and 295 K and the Ingalls' model does not apply. In contrast, a fit with a parabolic dependence given by $\Delta E_Q = \Delta E_{Q0}[1 - aT + bT^2]$ with $\Delta E_{Q0} = -2.228$ mm/s, $a = 2.02 \times 10^{-5}$ K^{-1}, and $b = -3.20 \times 10^{-7}$ K^{-2} is good. A successful fit with this empirical relationship indicates that the change in quadrupole interaction is dominated by the change in lattice parameters with increasing temperature.

Single Crystal Resistivity. The temperature dependence of the electrical resistivity measured along the *a*-axis in a $UFeSe_3$ single crystal between 2 and 300 K is shown in Figure 12. The resistivity decreases with increasing temperature suggesting semiconductor-like behavior. The resistivity at 297 K is 3.74×10^{-2} Ω cm, a value that is only slightly larger than the 2.5×10^{-2} Ω cm observed[46] for β-USe_2. Below 30 K the resistance of $UFeSe_3$ along the *a*-axis exceeded the capacity of the instrument, and all attempts to measure the resistance at lower temperatures using alternative methods also failed; this failure suggests that the resistivity is greater than 10^6 Ω cm. When the crystal is warmed from 30 to 50 K the resistivity decreases by 2 orders of magnitude from 16.4 to 0.093 kΩ cm.

A plot of ln(ρ) versus $1/T$ for $UFeSe_3$ is shown as the inset to Figure 12. The resistivity can be fit with the expression $\rho = \rho_0 \exp(\Delta E_{act}/k_B T)$, a fit that corresponds to an Arrhenius thermal activation process in which the activation energy, expressed as $\Delta E_{act}/k_B T$, corresponds to the band gap of a homogeneous semiconductor expressed as $E_g/2k_B T$. Unfortunately, the resistivity measured above 214 K exhibited a poor signal-to-noise ratio and was not included in the fits. The Arrhenius plot clearly exhibits three thermal regimes, 30 to 50, 50 to 107, and 107 to 214 K, for the activation energy. Note that 50 K is close to the 53 K maximum in the susceptibility along the *a*-axis, and 107 K is essentially the temperature of the shoulder-like feature in the magnetic susceptibility of $UFeSe_3$. For these three regimes, ΔE_{act} is 273(4) cm^{-1} or 0.0339(5) eV between 30 and 50 K, 387(2) cm^{-1} or 0.0480(2) eV between 50 and 107 K, and 236(4) cm^{-1} or 0.0293(4) eV between 107 and 214 K; the corresponding ρ_0 values are $39(5) \times 10^{-3}$, $1.36(4) \times 10^{-3}$, and $10.4(3) \times 10^{-3}$ Ω cm, respectively.

A change in resistivity below a magnetic ordering temperature has also been observed[47,48] in α-USe_2, β-USe_2, and USSe, but in these compounds the resistivity decreases rapidly in the magnetically ordered region. The temperature dependence of the resistivity of $UFeSe_3$ is closer to that observed for antiferromagnetic α-US_2, but in the latter compound the magnetic ordering induces an order of magnitude decrease in the band gap.[46] A semiclassical band model[46] with exchange interactions between conduction electrons and localized spins successfully explains the temperature dependence of the resistivity of α-US_2.

The percentage change in $(\rho_H - \rho_0)/\rho_0$, or $\Delta\rho/\rho_0$, where ρ_0 is the resistivity at zero applied field, observed for $UFeSe_3$ as a function of the magnetic field, *H*, applied perpendicular to *i* at temperatures both above and below 53 K, the temperature of the maximum in the susceptibility along the *a*-axis, is shown in the inset to Figure 13. $UFeSe_3$ exhibits a negative magnetoresistance that increases in magnitude with decreasing temperature between 60 and 35 K; the magnetoresistance is small at less than -0.5% at fields below 0.5 T. Because there is more than a 12% reduction in resistivity at 5 T, the temperature dependence of the resistivity between 2 and 100 K has been measured with the applied field perpendicular to *i* (see the main portion of Figure 13). At 60 K the magnetoresistance of $UFeSe_3$ becomes significant and reduces the resistivity; a maximum of 13% negative magnetoresistance was obtained at 34 K. Below this temperature the resistance of the material again exceeded the capability of the instrument. Above 60 K the magnetoresistance is minimal and does not exceed $\pm 1.5\%$. The measurements of $\Delta\rho/\rho_0$ are very sensitive to the value ρ_0 that is obtained at zero applied field, but unfortunately it is sometimes difficult to return the sample to an exact zero applied field. This difficulty accounts for why the magnetoresistances at 60 K and 5 T are negative in the inset to Figure 13 and positive or very close to zero in the main

(45) Ingalls, R. *Phys. Rev.* **1964**, *133*, A787–A795.
(46) Shlyk, L.; Troc, R. *Physica B* **1999**, *262*, 90–97.
(47) Shlyk, L.; Troc, R.; Kaczorowski, D. *J. Magn. Magn. Mater.* **1995**, *140−144*, 1435–1436.
(48) Troc, R.; Kaczorowski, D.; Shlyk, L.; Potel, M.; Noël, H. *J. Phys. Chem. Solids* **1994**, *55*, 815–823.

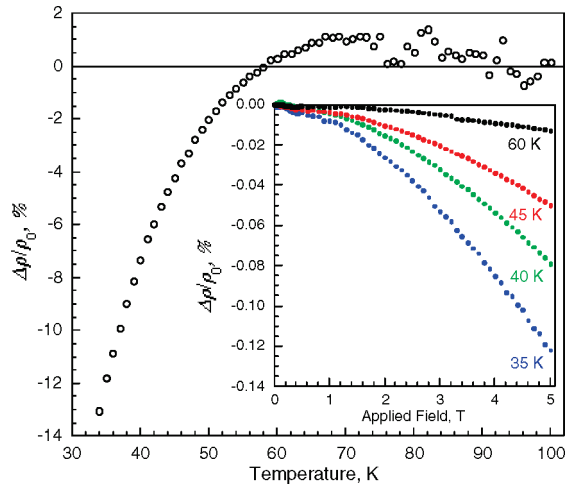

Figure 13. Temperature dependence of the percentage magnetoresistivity of $UFeSe_3$ obtained in a 5 T field applied perpendicular to the direction of the current. Inset: The percentage magnetoresistance obtained at the indicated temperatures.

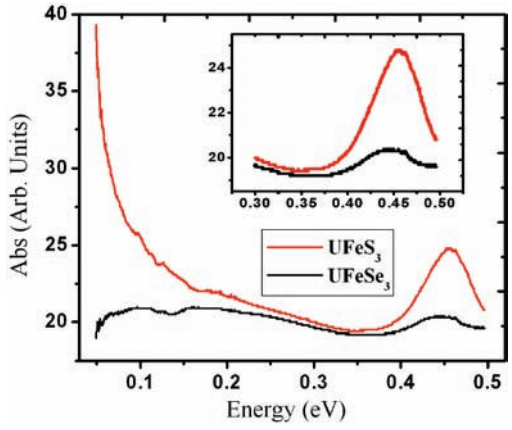

Figure 14. Infrared spectra of $UFeS_3$ and $UFeSe_3$.

portion of Figure 13. A reduction in the temperature dependence of the magnetoresistivity below the magnetic ordering temperature has also been observed[46] in antiferromagnetic α-US_2; however in this compound the magnetoresistance at low temperature is independent of the applied field. In α-USe_2 and β-USe_2 the magnetoresistance at low temperatures is field dependent, but unlike that observed in $UFeSe_3$ the magnetic alignment induces a semiconductor-to-semimetal transition.[47] The field dependence of the magnetoresistance of $UFeSe_3$ is most likely related to the ratio of magnetocrystalline anisotropy energy to the exchange interaction energy.[46]

Optical Properties. The diffuse reflectance spectra of $UFeS_3$ and $UFeSe_3$ are almost featureless over the range of 200 to 2500 nm, that is, from 6.21 to 0.50 eV. The infrared spectra of $UFeS_3$ and $UFeSe_3$ obtained between 0.05 to 0.50 eV, that is, from 400 to 4000 cm^{-1}, are shown in Figure 14. An absorption at about 0.45 eV is observed for both compounds; the nature of this absorption is unknown.

Magnetic Behavior of $UFeS_3$ and $UFeSe_3$. The temperature dependence of the magnetic susceptibility along the *a*- and *b*-axes, typically a broad maximum along the *a*-axis, a non-zero susceptibility at 0 K, and a smooth small decrease of the susceptibility along both axes as the temperature increases above 50 K, is characteristic[30] of two-dimensional magnetic compounds. The iron-57 Mössbauer spectra of both $UFeS_3$ and $UFeSe_3$ indicate either an ordering or slow fluctuations of the iron(II) magnetic moments at about 107 K, a temperature that is consistent with the shoulder-like anomalies observed in the molar magnetic susceptibility of $UFeSe_3$ when the field is applied parallel to the *a*- and *b*- axes. Both the Brillouin-like temperature dependence of the magnetic hyperfine field and the change in quadrupole splitting resulting from magnetostriction point[30] toward long-range magnetic ordering of at least the iron(II) magnetic moments below 107 K. Finally, the observation of magnetoresistance below about 50 K also indicates the presence of long-range magnetic ordering, an ordering that may, below 50 K, include the uranium(IV) magnetic moments. The linear field dependence of the magnetization and the field dependence of the magnetoresistance of $UFeSe_3$ indicate that the magnetocrystalline anisotropy and magnetic exchange energies are of the same order of magnitude.

Below about 100 K the Mössbauer spectra of both $UFeS_3$ and $UFeSe_3$ indicate that a magnetic transition occurs for the iron(II). However, the spectra cannot be analyzed with a single magnetic iron site as would be expected on the basis of the unique iron crystallographic site undergoing a magnetic transition. At least four magnetic components with different hyperfine field strength and orientations are required to satisfactorily fit the spectra, but four magnetically inequivalent iron sites could not be identified. Hence, we are forced to conclude that the four components model a double distribution of the hyperfine fields and probably the Euler θ angles; at least two parameters must be distributed in view of the line shape profile of the spectra. Such a distribution may result from a non-collinear arrangement of the iron(II) magnetic moments below about 107 K. For instance, a spiral or helical ordering of the iron(II) magnetic moments will result in a distribution of the hyperfine field strength and orientation. Note that there must be a weak superexchange interaction between the iron(II) ions that are about 3.8−3.9 Å apart along the *a*-axis and between which the Fe−*Q*−Fe exchange pathways have an angle of 135°, substantially smaller than the ideal 180° angle that would maximize the superexchange. The exchange between the *ac*-planes of iron(II) is even weaker through a successive stacking of a *Q* layer, a uranium(IV) layer, and a second *Q* layer along the *b*-axis. Hence, it is possible that between about 50 and 107 K, the iron(II) layers exhibit long-range magnetic ordering within the layer but not between the layers.

The iron-57 Mössbauer spectra remain essentially unchanged below about 40 K, that is, below the temperature at which the magnetic anisotropy changes and is dominated by uranium(IV). In $UFeS_3$ and $UFeSe_3$ the iron and uranium magnetic sublattices appear essentially independent of each other.

Conclusions

The $AnMQ_3$ compounds, where *An* is U or Th, *M* is a transition-metal cation, and *Q* is S, Se, or Te, show an interesting variety of physical properties, especially their magnetic properties, that involve different and complex

interactions among the actinide and transition-metal cations. Large single crystals of $UFeS_3$ and $UFeSe_3$ have been obtained through solid-state reactions in the presence of a CsCl flux. For each compound, the availability of single crystals has permitted a study of their single-crystal magnetic susceptibility. To the best of our knowledge this is the first single-crystal study of any of the physical properties of any of the $AnMQ_3$ compounds.

Both X-ray absorption and Mössbauer spectra of $UFeS_3$ and $UFeSe_3$ confirm the presence of high-spin iron(II) and uranium(IV). The temperature dependence of the electrical resistivity of a single crystal of $UFeSe_3$ has been measured along the *a*-axis. $UFeSe_3$ exhibits semiconductor character between 2 and 300 K with two energy gap transitions at about 50 and 107 K, changes that are associated with the maximum in the susceptibility measured along the *a*-axis and the shoulder-like feature in the susceptibility measured along the *a*- and *b*-axes. In $UFeSe_3$ a negative magnetoresistance has been observed below 60 K.

The compounds exhibit similar complex magnetic properties, as expected from the presence of two well-defined magnetic sublattices of iron(II) and uranium(IV) in the *ac*-plane separated by S or Se layers. Both compounds show a substantial magnetic anisotropy. Above about 40 K it is dominated by the iron(II) single ion anisotropy and the easy axis is along the *a*-axis, whereas below 40 K it is dominated by the uranium(IV) anisotropy and the easy axis is along the *b*-axis. The *c*-axis is the hard axis at all temperatures. The effective paramagnetic magnetic moments along the *a*- and *b*-axis agree with the presence of iron(II) and uranium(IV) cations. A small shoulder-like feature is observed at 96 and 107 K in the magnetic susceptibilities measured along the *a*- and *b*-axis, respectively. Finally, a broad maximum is observed at about 50 K in the magnetic susceptibility measured along the *a*-axis.

The iron-57 Mössbauer spectra of $UFeS_3$ and $UFeSe_3$ are paramagnetic doublets above about 107 K and reveal the presence of a static hyperfine field below this temperature. The temperature dependence of the hyperfine field follows a Brillouin-like function, and no change associated with the maximum of the susceptibility at 50 K is observed in the Mössbauer spectra.

Acknowledgment. We thank Dr. Christos Malliakas and Prof. Mercouri G. Kanatzidis for help with the use of their UV−vis−NIR and FT−IR spectrometers and Prof. N. Edelstein for helpful discussions during the course of this work. The research at Northwestern University was supported by the U.S. Department of Energy, Basic Energy Sciences, Biosciences, and Geosciences Division and Division of Materials Sciences and Engineering Grant ER-15522. Resistivity measurements were collected at the Northwestern Materials Research Science and Engineering Center, Magnet and Low Temperature Facility supported by the National Science Foundation (DMR05-20513). Fernande Grandjean acknowledges the Fonds National de la Recherche Scientifique, Belgium (Grants 9.456595 and 1.5.064.05) for financial support. Magnetic measurements were performed at the National High Magnetic Field Laboratory, which is supported by the National Science Foundation through Grant DMR-0084173 and the State of Florida. PNC/XOR facilities at the Advanced Photon Source and research at these facilities are supported by the U.S. Department of Energy, Basic Energy Sciences, a major facilities access grant from NSERC, the University of Washington, Simon Fraser University, the Pacific Northwest National Laboratory, and the Advanced Photon Source. Use of the Advanced Photon Source is also supported by the U.S. Department of Energy, Office of Science, Office of Basic Energy Sciences, under Contract DE-AC02-06CH11357.

Supporting Information Available: Details of the single-crystal magnetic measurements, the magnetic properties of $UFeS_3$, details of the analysis of the Mössbauer spectra, and the X-ray crystallographic files in CIF format for $UFeS_3$ and $UFeSe_3$. This material is available free of charge via the Internet at http://pubs.acs.org.